Three-Dimensional Lattice Kinetic Scheme and its Application to Simulate Incompressible Viscous Thermal Flows

Y. Peng, C. Shu* and Y. T. Chew

Department of Mechanical Engineering, National University of Singapore, 10 Kent Ridge Crescent, Singapore 119260.

Abstract. In this paper, the three-dimensional lattice kinetic scheme is presented to simulate incompressible viscous thermal flows. As compared with the standard LBM, the present scheme has the following good features. It can save the computer memory since there is no need to store the density distributions. Like the conventional NS solvers, the implementation of boundary conditions is straightforward since the dependent variables are the macroscopic flow parameters. The easy implementation of boundary conditions is a good property for solving three-dimensional flow problems. The present scheme is validated by simulating the three-dimensional natural convection in an air-filled cubical enclosure, which is heated differentially at two vertical side walls. The obtained numerical results compare very well with available data in the literature.

PACS: 47.11.+j, 47.15.-x

Key words: Lattice kinetic scheme, lattice Boltzmann method, three-dimensional, incompressible flow, natural convection, thermal flow.

1 Introduction

The lattice Boltzmann method (LBM) is an alternative numerical scheme for simulating viscous flows [1, 2]. It has been widely used in many kinds of complex flows such as the turbulent flow, multiphase flow and micro-flow [3]. It has the following good features: the linear convection operator in the phase space, the pressure calculated using an equation of state and the use of a minimal set of velocities in the phase space. Furthermore, it

*Corresponding author. *Email addresses:* `YPeng@odu.edu` (Y. Peng), `mpeshuc@nus.edu.sg` (C. Shu), `mpecyt@nus.edu.sg` (Y. T. Chew)

has the intrinsic feature of parallelism. The only variables for LBM are the density distributions. The mapping from the density distributions to the fluid variables is a straightforward summation. In contrast, the inverse mapping from the fluid variables to the density distributions is somewhat tricky to make, especially for the three-dimensional problem. However, on the boundaries, the macroscopic fluid variables, instead of the density distributions, are usually given as the boundary conditions. The inverse mapping has to be used on the boundaries. Different ways to make the inverse mapping form different methods to implement boundary conditions. The bounce-back rule for the boundary condition is the simplest way to impose on the solid wall. Particles that meet at a wall point are simply bounced back with a reverse direction. This rule leads to a non-slip boundary located at somewhere between the wall nodes and the adjacent fluid nodes [4]. It is found to be only the first order in the numerical accuracy at the boundaries [5, 6] and its serious shortcomings have been pointed out by Noble et al [7]. More sophisticated boundary conditions, which model the non-slip boundary exactly at the wall nodes, have been proposed by several authors [8, 9]. Among them, the consistent hydrodynamic boundary condition has been widely used in recent years. It calculates the unknown density distributions from the velocity boundary conditions and the density distributions of neighboring fluid nodes near the boundary. This requires that the unknown density distributions should not exceed the available number of equations for the density and momentum. For two dimensions, the number of available equations is three and it is four for three dimensions. However, for the general three-dimensional problems, the unknown density distributions usually exceed four, especially for the corner points. The supplementary rules have to be introduced. Chen et al. [10] proposed a new boundary condition using a second-order extrapolation scheme to obtain the unknown density distributions on the boundary. Bouzidi et al. [11] proposed a new scheme for wall boundary conditions. It uses the bounce-back rule and interpolation. Ginzburg and d'Humiéres [12] presented a general framework for several previously introduced boundary conditions, such as the bounce-back rule and the linear and quadratic interpolations, and designed boundary conditions for general flows which are third-order kinetic accurate. Starting from the well developed theory of boundary conditions for the continuous Boltzmann equation, Ansumali and Karlin [13] derived the boundary condition for the discrete set of velocities. Using this boundary condition, the Knudsen layer in the Kramers' problem is reproduced correctly for small Knudsen numbers.

As an alternative approach, the two-dimensional lattice kinetic scheme was proposed by Inamuro [14]. Similar idea was also proposed by Martys [15]. It is based on the idea that if the dimensionless relaxation time in the LBM with BGK model is set to unity, the macroscopic variables can be calculated without using density distributions and the scheme becomes very similar to the kinetic approach. By merging the LBM with kinetic scheme, the implementation of boundary conditions is very easy and straightforward since on the boundaries, only the macroscopic variables are needed as for the conventional NS solvers. This feature is very distinguished as compared with the conventional LBM when the flow problems with complex geometry are solved. In addition, it can

save much memory as compared with the standard LBM, because there is no need to store the density distributions. The original lattice kinetic scheme is limited to the two-dimensional uniform grids. Its extension to the arbitrary mesh for the two-dimensional flow problems was made by Peng et al. [16] using the idea of Taylor series expansion- and least squares- based method.

In practical applications, three-dimensional flows are often encountered. When the flow problems with curved boundaries are solved, the boundaries cannot be well defined when the uniform grids are used. Even when the flows are confined in the regular domain, non-uniform grid is preferred at high Reynolds or Rayleigh numbers. In order to meet these requirements and exploit the good feature of the lattice kinetic scheme in the implementation of boundary conditions, its extension to three dimensions and its applications on arbitrary meshes are necessary for its development into a competitive method.

In this paper, we extended the lattice kinetic scheme to the three-dimensional case and then apply it to simulate incompressible viscous thermal flows on the arbitrary mesh using the idea of Taylor series expansion- and least squares- based method. To validate the new lattice kinetic scheme in three dimensions on the arbitrary mesh, a numerical study of the three-dimensional natural convection in an air-filled cubical enclosure, which is heated differentially at two vertical side walls, is carried out. The test problem has many engineering applications, such as cooling of electronic devices, energy storage systems and compartment fires. The present results compare very well with available data in the literature.

2 Methodology

At first, we will give a description on the three-dimensional lattice kinetic scheme on the uniform grid. Then, we will further extend its use on the arbitrary mesh.

2.1 Three-dimensional lattice kinetic scheme

We will take the particle velocity model of D3Q15 as an example to illustrate the three-dimensional lattice kinetic scheme. The configuration of D3Q15 is shown in Fig. 1, and its velocities are defined as:

$$\boldsymbol{e}_\alpha = \begin{cases} 0 & \alpha=0, \\ (\pm1,0,0),(0,\pm1,0),(0,0,\pm1) & \alpha=1-6, \\ (\pm1,\pm1,\pm1) & \alpha=7-14. \end{cases} \quad (2.1)$$

The evolution equation for the density distribution $f_\alpha(x,t)$ with the particle velocity e_α can be written as

$$f_\alpha(\boldsymbol{x},t+\delta t) = f_\alpha(\boldsymbol{x}-\boldsymbol{e}_\alpha\delta t,t) - \frac{f_\alpha(\boldsymbol{x}-\boldsymbol{e}_\alpha\delta t,t) - f_\alpha^{eq}(\boldsymbol{x}-\boldsymbol{e}_\alpha\delta t,t)}{\tau}, \quad \alpha=0,1,\dots,N, \quad (2.2)$$
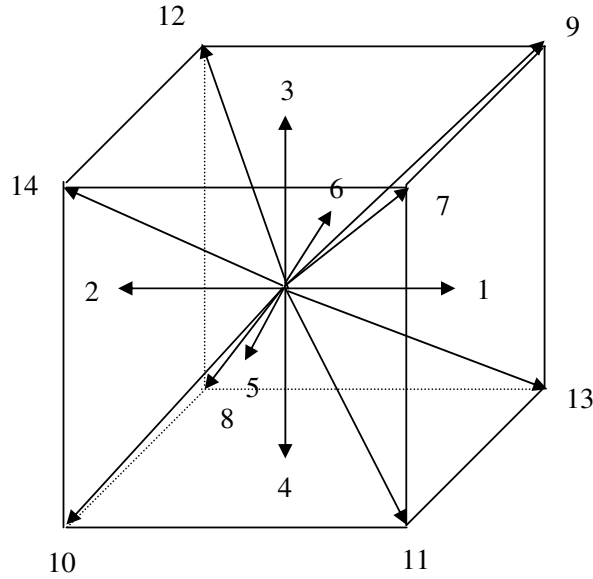
Figure 1: The lattice velocities of D3Q15.

where τ is the single relaxation time; f_α^{eq} is the corresponding density equilibrium distribution function; δt is the time step and N is the number of discrete particle velocities. On the uniform grid, δt is chosen so that the particles travel one-lattice spacing during this time. When D3Q15 is used, the equilibrium distribution function can be chosen as

$$f_\alpha^{eq} = w_\alpha \rho \left[1 + 3 e_\alpha \cdot V + \frac{9 (e_\alpha \cdot V)^2}{2} - \frac{3 V^2}{2} \right], \tag{2.3}$$

where $w_0 = 2/9$, $w_\alpha = 1/9$ for $\alpha = 1$-6 and $w_\alpha = 1/72$ for $\alpha = 7$-14. The macroscopic density ρ and fluid velocity V are calculated in terms of the density distributions as

$$\rho = \sum_{\alpha=0}^{14} f_\alpha, \qquad V = \frac{1}{\rho} \sum_{\alpha=0}^{14} f_\alpha e_\alpha. \tag{2.4}$$

The pressure p is computed from the equation of state by

$$p = \frac{\rho}{3} \tag{2.5}$$

and the kinematic viscosity v is given by

$$v = \frac{1}{3} \left(\tau - \frac{1}{2} \right) \delta t. \tag{2.6}$$

When the dimensionless relaxation time τ in equation (2.2) is set to unity, we can obtain

$$f_\alpha(\boldsymbol{x},t+\delta t) = f_\alpha^{eq}(\boldsymbol{x}-\boldsymbol{e}_\alpha\delta t,t). \tag{2.7}$$

Then using equation (2.3), we can get

$$\rho(\boldsymbol{x},t+\delta t) = \sum_{\alpha=0}^{14} f_\alpha^{eq}(\boldsymbol{x}-\boldsymbol{e}_\alpha\delta t,t),$$

$$\rho(\boldsymbol{x},t+\delta t)\,\boldsymbol{V}(\boldsymbol{x},t+\delta t) = \sum_{\alpha=0}^{14} f_\alpha^{eq}(\boldsymbol{x}-\boldsymbol{e}_\alpha\delta t,t)\boldsymbol{e}_\alpha. \tag{2.8}$$

By using equations (2.3) and (2.8), one can calculate the density and fluid velocity without using the density distributions. The pressure is obtained with equation (2.5) and the kinematic viscosity is given by

$$v = \frac{1}{6}\delta t. \tag{2.9}$$

This yields a very small time step at high Reynolds numbers. In order to remove this shortcoming, we modify f_α^{eq} to the following form [17]

$$f_\alpha^{eq} = w_\alpha\rho\left[1+3\boldsymbol{e}_\alpha\cdot\boldsymbol{V}+\frac{9(\boldsymbol{e}_\alpha\cdot\boldsymbol{V})^2}{2}-\frac{3V^2}{2}+A\delta t\left(\frac{\partial u_\delta}{\partial x_\gamma}+\frac{\partial u_\gamma}{\partial x_\delta}\right)e_{\alpha\delta}e_{\alpha\gamma}\right]. \tag{2.10}$$

There are other kinetic models proposed in [18–24]. By use of the Chapman-Enskog expansion or Grad's moment method, BGK-models with proper Prandtl number or being consistent with equilibrium thermodynamics can be derived.

In the same way, the lattice kinetic scheme for the temperature T is

$$T(\boldsymbol{x},t+\delta t) = \sum_{\alpha=0}^{14} g_\alpha^{eq}(\boldsymbol{x}-\boldsymbol{e}_\alpha\delta t,t) \tag{2.11}$$

with

$$g_\alpha^{eq} = w_\alpha T[1+3\boldsymbol{e}_\alpha\cdot\boldsymbol{V}]+w_\alpha B\delta t(\boldsymbol{e}_\alpha\cdot\nabla T). \tag{2.12}$$

By doing the Chapman-Enskog expansion, the following NS equation system can be obtained:

$$\nabla\cdot\boldsymbol{V}=0 \tag{2.13}$$

$$\frac{\partial\boldsymbol{V}}{\partial t}+(\boldsymbol{V}\cdot\nabla)\boldsymbol{V}=-\nabla p+v\nabla^2\boldsymbol{V} \tag{2.14}$$

$$\frac{\partial T}{\partial t}+(\boldsymbol{V}\cdot\nabla)T=\chi\nabla^2 T, \tag{2.15}$$

with the kinematic viscosity

$$v = \left(\frac{1}{6}-\frac{2}{9}A\right)\delta t, \tag{2.16}$$

and the thermal diffusivity

$$\chi = \left(\frac{1}{6} - \frac{1}{3} B \right) \delta t. \tag{2.17}$$

Note that in equations (2.10) and (2.12), the equilibrium distribution functions f^{eq} and g^{eq} can be calculated by using the particle velocities and macroscopic variables. Therefore, by using equations (2.8) and (2.11), one can calculate the macroscopic variables without using the density distributions. This can save a lot of memory space for the three-dimensional flows.

2.2　Three-dimensional lattice kinetic scheme on arbitrary mesh

In order to extend the use of three-dimensional lattice kinetic scheme on the arbitrary mesh, the idea of the Taylor series expansion and least squares optimization is introduced in the lattice kinetic scheme. The details of these techniques can be found in [25]. These techniques and their use in the standard LBM can be applied in the lattice kinetic scheme. It has been successfully tested on the two dimensional case [16]. In this paper, we will apply these techniques to the three dimensional case.

Suppose that the calculation point is at the grid point $P(x,y,z,t)$. As seen from equation (2.8), for the original lattice kinetic scheme, the macroscopic density and velocity can be calculated as the function of $f_\alpha^{eq}(x - e_{\alpha x}\delta t, y - e_{\alpha y}\delta t, z - e_{\alpha z}\delta t, t)$. For a uniform lattice, $\delta x = e_{\alpha x}\delta t$, $\delta y = e_{\alpha y}\delta t$, $\delta z = e_{\alpha z}\delta t$. So, $(x - e_{\alpha x}\delta t, y - e_{\alpha y}\delta t, z - e_{\alpha z}\delta t)$ is at the grid point and the values of $f_\alpha^{eq}(x - e_\alpha \delta t, t)$ can be easily determined from equation (2.10). In other words, equation (2.8) can be used to update the density and velocity exactly at the grid points. However, for a non-uniform grid, $(x - e_{\alpha x}\delta t, y - e_{\alpha y}\delta t, z - e_{\alpha z}\delta t)$ is usually not at the grid point $(x - \delta x, y - \delta y, z - \delta z)$. So the values of $f_\alpha^{eq}(x - e_\alpha \delta t, t)$ cannot be obtained from equation (2.10) directly since only the macroscopic properties such as the density and flow velocity at every mesh point are known. As a result, the density and velocity at the new time level cannot be obtained using equation (2.8). In order to get the values of $f_\alpha^{eq}(x - e_\alpha \delta t, t)$, the Taylor series expansion in the spatial direction is applied.

Let point P represent the calculation point (x_P, y_P, z_P, t), points Q_0 - Q_{14} represent the position $(x - e_{\alpha x}\delta t, y - e_{\alpha y}\delta t, z - e_{\alpha z}\delta t, t)$ and points P_1 - P_{14} represent the position $(x_{P_i}, y_{P_i}, z_{P_i}, t)$ with $x_{P_i} = x_P - \delta x_i$, $y_{P_i} = y_P - \delta y_i$, $z_{P_i} = z_P - \delta z_i$. So, equation (2.8) gives

$$\rho(x,t+\delta t) = \sum_{\alpha=0}^{14} f_\alpha^{eq}(x_\alpha, t),$$

$$\rho(x,t+\delta t) V(x,t+\delta t) = \sum_{\alpha=0}^{14} f_\alpha^{eq}(x_\alpha,t) e_\alpha, \tag{2.18}$$

where $x_0 = x_P$, $x_\alpha = x_{Q_\alpha}$, $\alpha = 1\text{-}14$.

For the general case, Q_1-Q_{14} may not coincide with the mesh points P_1-P_{14}. We will take the point Q_1 as an example. Q_1 may not coincide with the mesh point P_1. Since

$f_\alpha^{eq}(P_1,t)$ is known, we can build the connection between $f_\alpha^{eq}(Q_1,t)$ and $f_\alpha^{eq}(P_1,t)$ by using the Taylor series expansion to the second order derivative terms. That is

$$
\begin{aligned}
f_\alpha^{eq}(P_1,t) = {} & f_\alpha^{eq}(Q_1,t) + \Delta x_{P_1}\frac{\partial f_\alpha^{eq}(Q_1,t)}{\partial x} + \Delta y_{P_1}\frac{\partial f_\alpha^{eq}(Q_1,t)}{\partial y} + \Delta z_{P_1}\frac{\partial f_\alpha^{eq}(Q_1,t)}{\partial z} \\
& + \frac{1}{2}(\Delta x_{P_1})^2\frac{\partial^2 f_\alpha^{eq}(Q_1,t)}{\partial x^2} + \frac{1}{2}(\Delta y_{P_1})^2\frac{\partial^2 f_\alpha^{eq}(Q_1,t)}{\partial y^2} + \frac{1}{2}(\Delta z_{P_1})^2\frac{\partial^2 f_\alpha^{eq}(Q_1,t)}{\partial z^2} \\
& + (\Delta x_{P_1}\Delta y_{P_1})\frac{\partial^2 f_\alpha^{eq}(Q_1,t)}{\partial x\partial y} + (\Delta x_{P_1}\Delta z_{P_1})\frac{\partial^2 f_\alpha^{eq}(Q_1,t)}{\partial x\partial z} \\
& + (\Delta y_{P_1}\Delta z_{P_1})\frac{\partial^2 f_\alpha^{eq}(Q_1,t)}{\partial y\partial z} + \mathcal{O}[(\Delta x_{P_1})^3,(\Delta y_{P_1})^3(\Delta z_{P_1})^3],
\end{aligned}
\tag{2.19}
$$

where $\Delta x_{P_1} = x_{P_1} - (x_P - e_{\alpha x}\delta t)$, $\Delta y_{P_1} = y_{P_1} - (y_P - e_{\alpha y}\delta t)$, $\Delta z_{P_1} = z_{P_1} - (z_P - e_{\alpha z}\delta t)$. For the three-dimensional case, this expansion involves 10 unknowns, that is, one equilibrium distribution function at the point Q_1, three first order derivatives, and six second-order derivatives at the same point. To solve for these unknowns, 10 equations are needed to close the system. This can be done by building the connections with other mesh points, which is made by applying the second-order Taylor series expansion at the other 9 points: P_0, P_2 - P_9. The following equation system can be obtained:

$$
f_k' = \{s_k\}^T\{W\} = \sum_{j=0}^{9} s_{k,j}W_j, \qquad k = P_0\text{-}P_9,
\tag{2.20}
$$

where

$$
\begin{aligned}
& f_k' = f_\alpha^{eq}(x_k,y_k,z_k,t), \\
& \{s_k\}^T = \{1,\Delta x_k,\Delta y_k,\Delta z_k,(\Delta x_k)^2/2,(\Delta y_k)^2/2,(\Delta z_k)^2/2,\Delta x_k\Delta y_k,\Delta x_k\Delta z_k,\Delta y_k\Delta z_k\}, \\
& \{W\} = \{f_\alpha^{eq},\partial f_\alpha^{eq}/\partial x,\partial f_\alpha^{eq}/\partial y,\partial f_\alpha^{eq}/\partial z,\partial^2 f_\alpha^{eq}/\partial x^2,\partial^2 f_\alpha^{eq}/\partial^2 y,\partial^2 f_\alpha^{eq}/\partial^2 z, \\
& \qquad \partial^2 f_\alpha^{eq}/\partial x\partial y,\partial^2 f_\alpha^{eq}/\partial x\partial z,\partial^2 f_\alpha^{eq}/\partial y\partial z\}^T.
\end{aligned}
$$

Our target is to find the first element $W_1 = f_\alpha^{eq}(Q_1,t)$. Equation system (2.20) can be put into the following matrix form

$$
[S]\{W\} = \{f'\},
\tag{2.21}
$$

where $[S]$ is a matrix formed by the vector $\{s_k\}$. In practical applications, it was found that the matrix $[S]$ might be singular or ill-conditioned using only ten points (P_0 - P_9). To overcome this difficulty and make the method be more general, more points are added and the least squares optimization [26] was introduced to optimize the over-constrained approximation by equation (2.21). As a result, the equation system for $\{W\}$ becomes

$$
\{W\} = \left([S]^T[S]\right)^{-1}[S]^T\{f'\} = [A]\{f'\}.
\tag{2.22}
$$

From equation (2.22), we can have

$$f_\alpha^{eq}(Q_1,t) = W_1 = \sum_{k=0}^{M-1} a_{1,k} f_k', \tag{2.23}$$

where $a_{1,k}$ are the elements of the first row of the matrix $[A]$, which is determined by the coordinates of the mesh points, the particle velocity and time step size, and will not be changed in the calculation procedure, M is the number of the points used and should be greater than 10. In the present study, a structured grid is used, and M is taken as 15. This means that for a reference mesh point P, we need to select its fourteen neighboring points to compute the coefficients in equation (2.23). The above procedure shows the calculation of $f_\alpha^{eq}(Q_1,t)$ and the same procedure can be applied to calculate the equilibrium distribution function at other points such as Q_0, Q_2 - Q_{14}. Then the density and velocity can be obtained by

$$\rho(\boldsymbol{x},t+\delta t) = \sum_{Q_0-Q_{14}} \sum_{k=0}^{M-1} a_{1,k} f_k',$$
$$\rho(\boldsymbol{x},t+\delta t)\boldsymbol{V}(\boldsymbol{x},t+\delta t) = \sum_{Q_0-Q_{14}} \sum_{k=0}^{M-1} a_{1,k} f_k' \boldsymbol{e}_\alpha. \tag{2.24}$$

We can calculate the coefficients in equation (2.24) once and store them in advance, so little computational effort is introduced as compared with the original lattice kinetic scheme. On the other hand, equation (2.24) is nothing to do with the mesh structure. It only needs the information on coordinates of the mesh points. Thus, we can say that equation (2.24) can be consistently used to any kind of mesh structure. On the other hand, we have to indicate that, as compared to the original lattice kinetic scheme, the present method requires much more memory to store the coefficients $a_{1,k}$. This is the price paid for its application to the arbitrary mesh.

The same procedure can be applied to the calculation of $g_\alpha^{eq}(\boldsymbol{x}-\boldsymbol{e}_\alpha\delta t,t)$ so that the temperature can be obtained. If we use the same particle velocity model and neighboring points, the geometry matrix for $g_\alpha^{eq}(\boldsymbol{x}-\boldsymbol{e}_\alpha\delta t,t)$ is the same as for $f_\alpha^{eq}(\boldsymbol{x}-\boldsymbol{e}_\alpha\delta t,t)$, which can save the computational time and memory space. The temperature can be obtained by

$$T(\boldsymbol{x},t+\delta t) = \sum_{Q_0-Q_{14}} \sum_{k=0}^{M-1} a_{1,k} g_k', \tag{2.25}$$

where $g_k' = g_\alpha^{eq}(x_k,y_k,t)$.

The equation systems (2.10), (2.16), (2.24) for the density, velocity and (2.12), (2.17), (2.25) for the temperature form our new three-dimensional lattice kinetic scheme on the arbitrary mesh.

As seen from equations (2.10) and (2.12), there exist velocity and temperature gradients, which are needed to be calculated by the finite-difference technique.
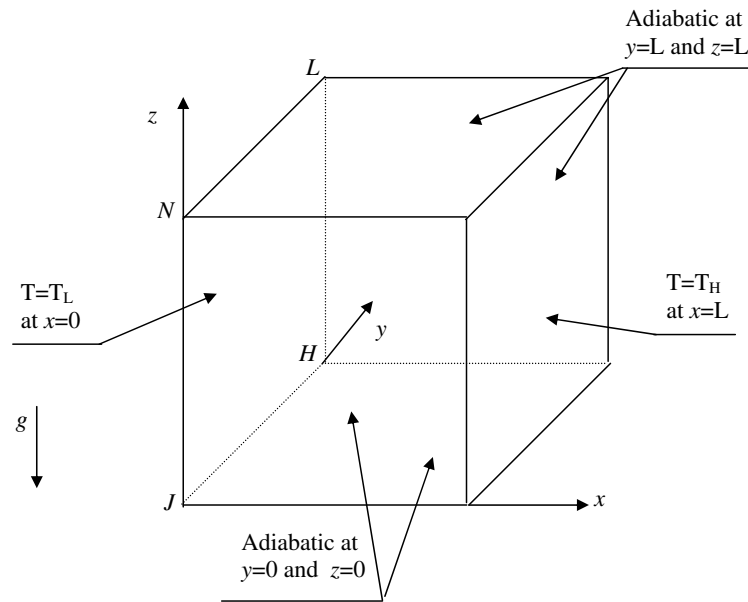
Figure 2: Configuration of the natural convection in a cubical cavity.

3 Implementation of boundary conditions

On the boundaries, usually the macroscopic variables and their first order derivatives are specified. These conditions can be implemented directly for the lattice kinetic scheme in the same way as for the conventional computational fluid dynamics (CFD) solvers. This is one of the attractive advantages of the lattice kinetic scheme over the standard LBM as pointed out in the introduction. In order to illustrate this, we will take the left vertical wall of a cubic enclosure as an example. Suppose that *HJNL* as shown in Fig. 2 is the left vertical wall for the flow configuration. For the conventional LBM, at the boundary line *HJ*, the density distributions at the directions 1, 5, 7, 9, 10, 11, 13 and 14 are unknowns. The number of the unknown density distributions exceeds 4, so the consistent hydrodynamic boundary condition cannot be directly used. Usually, the bounce-back rule of the non-equilibrium distribution proposed by Zou and He [27] can be used. So the density distributions at the directions 1, 5, 7 and 11 can be determined from the boundary condition. However, the two density distributions at the directions 9, 10, 13 and 14 are still not determined. Assumptions have to be introduced. When Neumann boundary conditions are encountered, things become more complicated. However, for the lattice kinetic scheme, on the boundaries, the given macroscopic variables and their first order derivatives can be implemented directly. There is no need to make any assumption or introduce any supplementary condition.

4   Numerical simulation

In order to validate the application of the lattice kinetic scheme in the three dimensional case, the computations for a sample problem are carried out. The problem considered is a natural convection in a three-dimensional cubical cavity with two vertical side walls maintained at different temperatures. The temperature difference between the walls introduces a temperature gradient in a fluid, and the consequent density difference induces the fluid motion, that is, convection. The remaining walls are adiabatic. The definition of this problem and boundary conditions are displayed in Fig. 2.

4.1   Buoyancy force and dimensionless parameters

The Boussinesq approximation is applied to the buoyancy force term. This means that the properties β and v are considered as constants, the density ρ is constant, and the buoyancy term is assumed to depend linearly on the temperature,

$$\rho\boldsymbol{G} = \rho\beta g_0(T - T_m)\boldsymbol{k}, \tag{4.1}$$

where β is the thermal expansion coefficient; g_0 is the acceleration due to gravity; $T_m = (T_H + T_L)/2$ is the average temperature, in which T_L and T_H are low and high temperatures on the side walls, respectively; $\boldsymbol{k}$ is the vertical direction opposite to that of the gravity. Correspondingly, the external force term $3w_\alpha g\beta(T - T_m)e_{\alpha z}\delta t$ is added to the density equilibrium distribution function (2.10).

The dimensionless parameters for this natural convection problem are Prandtl number Pr and Rayleigh number Ra defined by

$$Pr = v/\chi \tag{4.2}$$

$$Ra = \frac{\beta\Delta T g_0 L^3}{v\chi}, \tag{4.3}$$

where $\Delta T = T_H - T_L$ and L is the height of the cubic cavity.

In equation (4.3), $\sqrt{\beta g_0 \Delta T L}$ is the characteristic velocity. To ensure the code working properly in the near-incompressible regime, the value of $\sqrt{\beta g_0 \Delta T L}$ should be carefully chosen. It is chosen to be 0.1 at low Rayleigh numbers and 0.15 at high Rayleigh numbers. This means that the Mach number is 0.1 at low Rayleigh numbers and 0.15 at high Rayleigh numbers.

Once the two dimensionless parameters Pr and Ra are given, the kinematic viscosity and thermal diffusivity are determined by solving equations (4.2) and (4.3). Then the two parameters A and B in equations (2.10) and (2.12) can be determined through the relationships expressed by equations (2.16) and (2.17).

The Nusselt number Nu is one of the most important dimensionless parameters in describing the convective heat transport. The Nusselt numbers at the isothermal walls
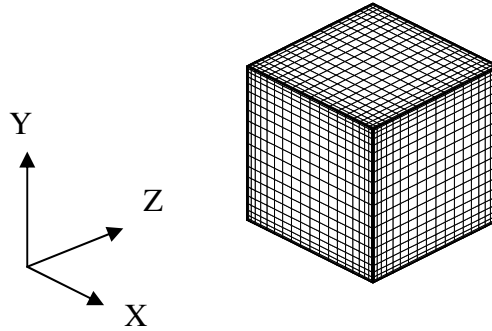
Figure 3: Typical non-uniform mesh system of a cubic cavity.

are defined as

$$Nu_{mean}(y) = \int_0^1 \left. \frac{\partial T(y,z)}{\partial x} \right|_{x=0 \text{ or } x=1} dz \tag{4.4}$$

$$Nu_{overall} = \int_0^1 Nu_{mean}(y)\,dy. \tag{4.5}$$

4.2   Grid and convergence criterion

In the present simulation, a non-uniform grid is used. The grid size used is $101 \times 101 \times 101$. The non-uniform grid is formed by stretching the mesh points near the walls, which is shown in Fig. 3. The time step is the minimum grid distance. The convergence criterion for all the cases is set to

$$\max_{i,j,k} \left| \sqrt{(u^2+v^2+w^2)^{n+1}} - \sqrt{(u^2+v^2+w^2)^n} \right| \leq 10^{-7},$$

$$\max_{i,j,k} \left| T^{n+1} - T^n \right| \leq 10^{-7}, \tag{4.6}$$

where n and $n+1$ represent the old and new time levels, respectively.

4.3   Validation of the numerical results and analysis of flow and thermal fields

Numerical simulations of the natural convection in a cubic cavity at Rayleigh numbers of 10^3 to 10^5 are carried out. Table 1 shows the representative quantities of the flow field and the heat transfer rates in the symmetry plane ($y=0.5$). The overall Nusselt number on the isothermal wall of $x=0$ for each Rayleigh number is also shown in this table. The numerical results of an N-S solver using a high-resolution finite difference method [28] are included for comparison.

Table 1: Comparison of the representative field parameters between the present lattice kinetic scheme and a Navier-Stokes solver [28].

Ra	10^3		10^4		10^5	
Method	Present	NS solver	Present	NS solver	Present	NS solver
u_{max}	0.132	0.1314	0.207	0.2013	0.147	0.1468
z	0.180	0.2000	0.170	0.1833	0.150	0.1453
v_{max}	0.133	0.1320	0.219	0.2252	0.250	0.2471
x	0.820	0.8333	0.880	0.8833	0.930	0.9353
Nu_{max}	1.420	1.420	3.630	3.652	7.89	7.795
z	0.090	0.08333	0.162	0.1623	0.09	0.08256
Nu_{min}	0.750	0.7639	0.600	0.6110	0.80	0.7867
z	1.0	1.0	1.0	1.0	1.0	1.0
Nu_{mean}	1.098	1.105	2.297	2.302	4.659	4.646
$Nu_{overall}$	1.076	1.085	2.088	2.100	4.378	4.361

In the symmetry plane of $y = 0.5$, the representative quantities of the flow field include: the maximum horizontal velocity u_{max} on the vertical mid-line in this plane and its location z, the maximum vertical velocity v_{max} on the horizontal mid-line and its location x. The representative quantities of the heat transfer rates in this symmetry plane contain the following Nusselt numbers defined at the vertical boundary $x = 0$. They are: the maximum value of the local Nusselt number Nu_{max} and its location z, the minimum value of the local Nusselt number Nu_{min} and its location z, and the average Nusselt number Nu_{mean}. The grid size of $32 \times 32 \times 32$ is used for $Ra = 10^3$, $64 \times 64 \times 64$ for $Ra = 10^4$ and $Ra = 10^5$ by the NS solver. From the table, we can see that the numerical results using the present three-dimensional lattice kinetic scheme agree very well with the benchmark data. There are little differences between some representative quantities. This shows that the three-dimensional lattice kinetic scheme has the capability for the real thermal applications.

The streamlines and isotherms in the symmetry plane of $y = 0.5$ for $Ra = 10^3$ to $Ra = 10^5$ are shown in Figs. 4 to 6. They compare well with the contours obtained by Sivaloganathan using the pseudospectral method [29]. They are qualitatively similar to those in the two-dimensional thermal cavity. However, the three dimensional effect is notable and it can be represented in the overall Nusselt number at the isothermal walls, which is to be described in the following section.

4.4   The overall Nusselt number at the isothermal walls

The non-dimensional heat transfer rate on the isothermal walls is a very important parameter in the engineering application. From Table 1, we can see that for $Ra = 10^3$, the overall Nusselt number at the heated wall is 1.076, while for the two-dimensional square cavity, the average Nusselt number on the heated wall is 1.117. The three-dimensional
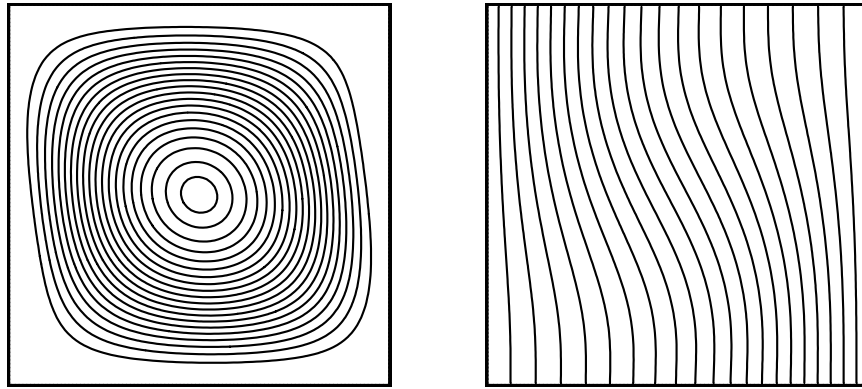
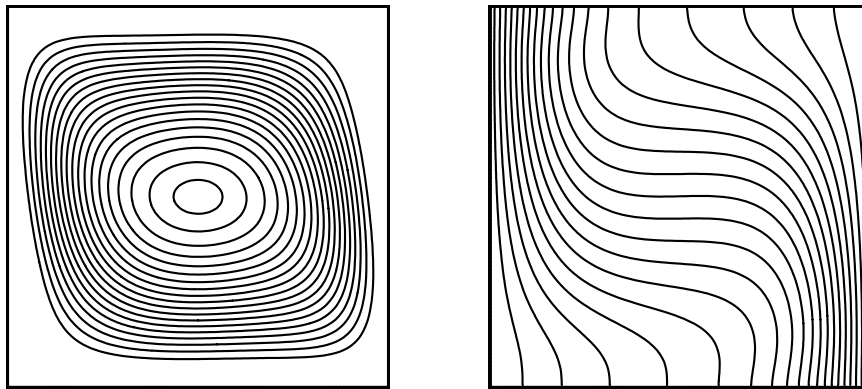Figure 4: Streamlines and isotherms for $Ra=10^3$ in a cubical cavity $(y=0.5)$.

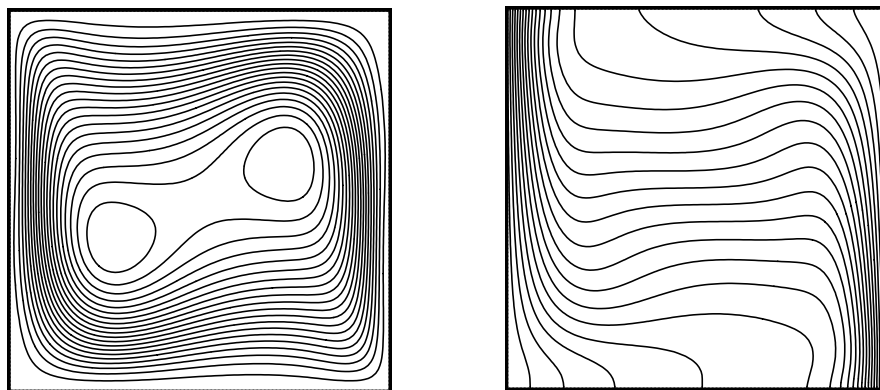Figure 5: Streamlines and isotherms for $Ra=10^4$ in a cubical cavity $(y=0.5)$.

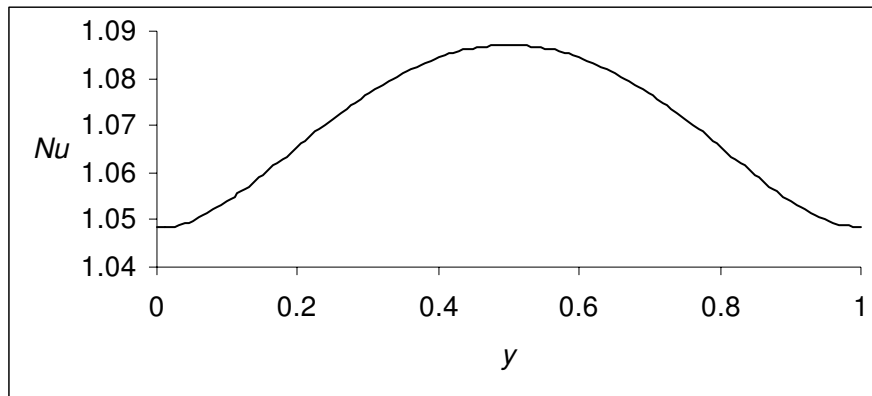Figure 6: Streamlines and isotherms for $Ra=10^5$ in a cubical cavity $(y=0.5)$.

Figure 7: Distribution of the mean Nusselt number in the y-direction for $Ra = 10^3$.

result of the overall Nusselt number is smaller than that in two dimensions, which shows the effect of the side walls. This observation agrees well with the results shown in Fig. 7. Fig. 7 represents the profile of the mean Nusselt number along the y-direction on the heated wall of $x = 0$ for $Ra = 10^3$. The mean Nusselt number increases as the symmetry plane is approached, and its peak value occurs at the symmetry plane located at $y = 0.5$. The peak value at the symmetry plane is still smaller than the two-dimensional average Nusselt number. So the overall Nusselt number should be smaller than the two-dimensional result. The same trend is applied to $Ra = 10^4$ and $Ra = 10^5$.

5   Conclusions

The lattice kinetic scheme is successfully extended and applied to the three-dimensional incompressible viscous thermal flows on the arbitrary mesh. The present scheme uses the macroscopic flow parameters such as density, velocity and temperature as dependent variables. The numerical results of the three-dimensional natural convection in an air-filled cubical enclosure obtained by present scheme agree well with the available benchmark data. It shows that the proposed scheme is very suitable for the practical applications.

References

[1] F. J. Higuera, S. Succi and R. Benzi, Lattice gas-dynamics with enhanced collisions, Europhys. Lett., 9 (1989), 345-349.
[2] Y. H. Qian, D. Dhumieres and P. Lallemand, Lattice BGK models for Navier-Stokes equation, Europhys. Lett., 17 (1992), 479-484.
[3] S. Chen and G. D. Doolen, Lattice Boltzmann method for fluid flows, Annu. Rev. Fluid Mech., 30 (1998), 329-364.

[4] X. He, Q. Zou, L. S. Luo and M. Dembo, Analytic solutions of simple flows and analysis of nonslip boundary conditions for the lattice Boltzmann BGK model, J. Stat. Phys., 87 (1997), 115-136.

[5] P. Lallemand and L. S. Luo, Theory of the lattice Boltzmann method: Dispersion, dissipation, isotropy, Galilean invariance and stability, Phys. Rev. E, 61 (2002), 6546-6562.

[6] R. Cornubert, D. d'Humiéres and D. Levermore, A Knudsen layer theory for lattice gases, Physica D, 47 (1991), 241-259.

[7] R. Noble, S. Chen, J. G. Georgiadis and R. O. Buckius, A consistent hydrodynamic boundary condition for the lattice Boltzmann method, Phys. Fluid, 7 (1995), 203-209.

[8] P. Skordos, Initial and boundary condition for the lattice Boltzmann method, Phys. Rev. E, 48 (1993), 4823-4842.

[9] R. Maier, R. Bernard and D. W. Grunau, Boundary conditions for the lattice Boltzmann method, Phys. Fluid, 8(7) (1996), 1788-1801.

[10] S. Chen, D. Martinez and R. Mei, On boundary conditions in lattice Boltzmann methods, Phys. Fluids, 8 (1996), 2527-2536.

[11] M. Bouzidi, M. Firdaouss and P. Lallemand, Momentum transfer of a Boltzmann-lattice fluid with boundaries, Phys. Fluid, 13 (2001), 3452-3459.

[12] I. Ginzburg and D. d'Humiéres, Multireflection boundary conditions for lattice Boltzmann models, Phys. Rev. E, 68 (2003), 066614.

[13] S. Ansumali and I. V. Karlin, Kinetic boundary conditions in the lattice Boltzmann method, Phys. Rev. E, 66 (2002), 026311.

[14] T. Inamuro, A lattice kinetic scheme for incompressible viscous flows with heat transfer, Philos. T. Roy. Soc. A, 360 (2002), 477-484.

[15] N. Martys, A classical kinetic theory approach to lattice Boltzmann simulation, Int. J. Mod. Phys. C, 12 (2001), 1169-1178.

[16] Y. Peng, C. Shu, Y. T. Chew and T. Inamuro, A lattice kinetic scheme for the incompressible viscous thermal flows on arbitrary meshes, Phys. Rev. E., 69 (2004), 016703.

[17] S. Succi, The Lattice Boltzmann Equation for Fluid Dynamics and Beyond, Oxford University Press, Padstow, UK, 2001, pp. 62-63.

[18] H. Struchtrup, The BGK-model with velocity-dependent collision frequency, Cont. Mech. Thermodyn., 9(1) (1997), 23-32.

[19] L. Mieussens and H. Struchtrup, Numerical solutions for the BGK-Model with velocity-dependent collision frequency, in: Symposium on Rarefied Gasdynamics 23, AIP Conference Proceedings 663, 2003, pp. 320-327.

[20] J. W. Dufty, Kinetic theory and hydrodynamics for a low density granular gas, Adv. Complex Sys., 4 (2001), 397-406.

[21] I. V. Karlin, Exact summation of the Chapman-Enskog expansion from moment equations, J. Phys. A: Math. Gen., 33 (2000), 8037-8046.

[22] S. Ansumali, I. V. Karlin and H. C. Öttinger, Minimal entropic kinetic models for hydrodynamics, Europhys. Lett., 63 (2003), 798-804.

[23] C. D. Levemore, Moment closure hierarchies for kinetic theories, J. Stat. Phys., 5-6 (1996), 1021-1065.

[24] P. Andries, P. L. Tallec, J. P. Perlat and B. Perthame, The Gaussian-BGK model of Boltzmann equation with small Prandtl number, Eur. J. Mech. B Fluids, 19 (2000), 813-830.

[25] C. Shu, Y. T. Chew and X. D. Niu, Least square-based lattice Boltzmann method: A meshless approach for simulation of flows with complex geometry, Phys. Rev. E., 64 (2001), 045701.

[26] G. H. Golub and C. F. Van Loan, Matrix Computations, 3rd Ed., Johns Hopkins University

Press, Maryland, USA, 1996.

[27] Q. Zou and X. He, On pressure and velocity boundary conditions for the lattice Boltzmann BGK model, Phys. Fluids., 9 (1997), 1591-1598.

[28] F. Fusegi, J. M. Hyun, K. Kuwahara and B. Farouk, A numerical study of three-dimensional natural convection in a differentially heated cubical enclosure, Int. J. Heat Mass Tran., 34(6) (1991), 1543-1557.

[29] S. Sivaloganathan and A. Karageorghis, Numerical solution of the 3-D Buoyancy driven cavity problem by a pseudospectral method, App. Math. Comp., 75 (1996), 43-58.